Materials and Structures (2024)57:15
https://doi.org/10.1617/s11527-023-02274-x

ORIGINAL ARTICLE

Influence of thermal strain on concrete spalling

André Klimek · Ludwig Stelzner · Sascha Hothan · Jochen Zehfuß

Received: 4 May 2023 / Accepted: 29 October 2023

Abstract Understanding the susceptibility to spalling of concrete members in case of fire is important to evaluate the residual load-bearing capacity. The investigations of the spalling phenomenon of a concrete mixture using real scale members are necessary but expensive to carry out. Reducing the specimen size leads to an increase of boundary effects that can result in a reduced spalling or absence of spalling. In this study, fire tests were carried out on unrestrained, single-sided exposed, cuboid shaped specimens (0.6 m × 0.6 m × 0.29 m) as well as unrestrained and steel ring restrained cylindrical specimens (Ø = 0.47 m, h = 0.29 m), which induce different boundary conditions. These fire tests were carried out on two ordinary concrete mixtures. The two mixtures differ only in the type of aggregates (quartz gravel and basalt grit) and were used to investigate the influence of the thermal expansion of the aggregate on the spalling behaviour of the concrete. The results show a significant increase of the spalling depth due to the restrained thermal expansion achieved by the applied steel rings. Additionally, the type of aggregate has a direct influence on the spalling behaviour of a concrete mixture. The reduction of the boundary effects by the steel rings recreate the test conditions in the centre of a large concrete member. Thus, this type of specimen is suitable to determine the susceptibility to spalling of a material (screening-tests) as preliminary investigations to full scale fire tests.

Keywords Spalling · Concrete · Fire test · Restraint · Screening test

1 Introduction

Concrete is a versatile building material in civil engineering with varying ingredients and compositions. This variety differs the damage prediction of a concrete member in case of fire [1]. Thermohydraulic and thermomechanical damage mechanisms occur simultaneously and induce stresses inside the concrete member. These stresses are released in form of cracking. A local accumulation of cracks in the boundary zone of the fire exposed surface can result in spalling of concrete fragments, which leads to a reduced load-bearing cross-section of the member.

A. Klimek · L. Stelzner (✉) · S. Hothan
Bundesanstalt für Materialforschung und -prüfung, Unter den Eichen 87, 12205 Berlin, Germany
e-mail: ludwig.stelzner@bam.de

A. Klimek
e-mail: a.klimek@tu-braunschweig.de

S. Hothan
e-mail: sascha.hothan@bam.de

A. Klimek · J. Zehfuß
Institut für Baustoffe, Massivbau und Brandschutz (iBMB), Technische Universität Braunschweig, Beethovenstraße 52, 38106 Braunschweig, Germany
e-mail: j.zehfuss@ibmb.tu-bs.de

Published online: 08 January 2024

The thermohydraulic damage mechanism depends on the bound water and the structural density of the concrete. In case of fire, the dehydrating cement matrix shrinks and cracks occur [2] in the boundary zone of the fire exposed surface. Based on a theoretical approach of Harmathy [3], Stelzner et al. [4] experimentally showed a pressure-induced mass transport of water towards deeper parts of the concrete as well as the condensation of water in larger pores. Due to the low thermal conductivity of the concrete, a temperature gradient leads to a condensation and accumulation of the steam in cooler regions. The steady steam flow and the condensation form a saturated and impermeable zone for vapour [5] (”moisture clog” [3]). Additionally, Jansson [6] concluded, that the moisture content primarily has an effect on the mechanical properties in a critical zone. Thus, the increasing pore pressure in front of the saturated zone increases the formation of cracks and can lead to spalling. Thermomechanical damage is a result of a differently pronounced expansion of the concrete member due to the temperature gradient and stiffness of the material. The thermal expansion depends on the type and grain size of the aggregates in the concrete mixture. Schneider [7] shows a significant higher thermal expansion of concrete specimens containing quartzitic or calcareous aggregates compared to specimens that included basaltic aggregates. Quartz-containing aggregates in particular have a high volume increase of 0.8 % [8] due to the conversion of the mineral at 573 °C. In case of fire, the restraint of the continuously expanding aggregates by means of the stiffness of the concrete member lead to compressive stresses parallel to the fire exposed surface and tensile stresses perpendicular to the fire exposed surface. At the same time, the compressive and tensile strength of the concrete decrease significantly [9]. Bošnjak et al. [10] show a reduction of compressive strength of 55 % and 80 % of tensile strength for normal concrete at a temperature of 800 °C compared to the specimens at 20 °C. These thermomechanical induced stresses are reduced by the appearance of cracks, which can lead to spalling on the fire exposed surface. The prior described damage mechanisms and their expression depend mainly on the composition of the concrete member. Additionally, external factors, i.e. specimen size, restrained expansion and loading, influence the damage mechanisms as well as the spalling behaviour on the macroscopic scale. Investigating the susceptibility to spalling of a concrete mixture for one specimen size has advantages and disadvantages. Full-scale tests [11–14] are necessary to investigate the damage behaviour of a concrete under real load conditions, but these tests are expensive to carry out. Small scale tests on cubes or cylinders [15–17] are easier to perform, but the influence of boundary effects is high. Due to the small specimen size, cracks connect the fire exposed surface and the unexposed side of the specimen. Vaporised water escapes through these cracks from deeper parts of the specimen and thermohydraulic stresses are reduced as-well. Thus, the susceptibility to spalling is low for small scale concrete specimens. Different comparative multi-scale studies examined the spalling behaviour of small scale specimens, intermediate scale beams, intermediate scale cylinders and full scale slabs. Multi-scale studies for unrestrained specimens showed that if a full scale specimen of a concrete mixture was affected by spalling, the intermediate scale specimens also spalled, but to a lesser extend [18–20]. As for the small scale specimens, the spalling behaviour on the fire exposed surface of the intermediate scale specimens is also affected by boundary effects [21, 22]. Boström et al. [23] showed that adding uniaxial compressive stress (2.5 MPa) to cuboid shaped, intermediate scale specimens (0.6 m × 0.5 m × 0.2 m and 0.4 m × 0.4 m × 0.1 m) spalling increases compared to unloaded specimens of the same mixture and size. The external compressive stress led to a reduction of cracks and therefore, a reduction of the water loss at the sides of the specimen. Additionally, the authors showed that spalling occurred for small cylinders (Ø = 0.15 m; h = 0.3 m) if compressive stress (5.3 MPa) was applied. Thus, the addition of compressive stress increased the spalling volume independently of the specimen size and shape. Ozawa et al. [24] adapted the idea of reducing boundary effects by applying two steel rings on cylindrical shaped intermediate scale specimens (Ø = 0.3 m; h = 0.1 m). The steel rings were shadowed from a direct heat input of the furnace. Thus, the thermal expansion of the steel rings was lower compared to the concrete. The restrained thermal expansion of the specimen induced thermomechanical stresses inside the concrete during the fire tests. Additionally, the cylindrical shape allowed a more homogeneous expansion of the

specimen compared to cuboid shaped specimens and therefore, an easier stress determination. Three different high-performance concrete (HPC) mixtures with different coarse aggregates (limestone, tuff and sandstone) with and without polypropylene fibres (PP-fibres) were tested. The use of PP-fibres has a positive effect on the spalling behaviour of HPC [25–27]. Strain gauges were applied on the surface of the steel rings in several depths from the fire exposed surface. Afterwards, the restrained stresses inside the concrete were calculated by the strain measurements and the mechanical properties of the steel rings. The restrained stresses induced by the steel rings were larger for concrete mixtures with PP-fibres within the first 10 min of the fire test compared to specimens without PP-fibres. The increased spalling behaviour of the mixtures without PP-fibres led to short periods of stress release. Additionally, the spalling was influenced by the type of aggregate in the mixtures. The mixture with limestone showed greater spalling depths compared to the mixtures with tuff or sandstone. Thus, aggregates with low porosity (limestone) increase spalling and showed higher restrained stresses compared to aggregates with a higher porosity (sandstone, tuff [28]). Based on the investigations of Ozawa et al. [24], Mohaine et al. [29] carried out a study of single-sided fire exposed and restrained concrete specimens to investigate the spalling behaviour for different specimen sizes and shapes. Steel rings were applied to two cylindrical shaped specimens (Ø = 0.3 m; h = 0.11 m and Ø = 0.61 m; h = 0.3 m) and compared to unrestrained and uniaxial loaded (0.75 MPa) full scale specimens (1.7 m × 0.98 m × 0.2 m) of the same mixture. The results show a similar spalling behaviour of the uniaxial loaded full scale specimen (spalling depth: 105 mm) and the large cylindrical shaped specimens (spalling depth: 144 mm and 114 mm). The small (Ø = 0.3 m; h = 0.11 m) cylindrical shaped specimens showed little to no spalling. Thus, smaller specimens can represent the spalling behaviour of larger specimens for the same mixture if the specimens are restrained and the boundary effects reduced. The authors also showed a limitation to the reduction of the specimen size for a comparison of the spalling behaviour.

Based on these, previous observations, the fire tests presented in this study continue the investigation on the susceptibility to spalling of two ordinary concrete mixtures from a previous multi-scale study [18]. The aim of this project was the improvement of the type of specimen to reduce the boundary effects and recreate the test conditions in the centre of the full scale specimens of the same mixture.

2 Materials

2.1 Test set-up

The fire tests for all specimens were carried out in a special furnace, developed for research purposes with a volume of one m^3, the so-called one-m^3 furnace. Figure 1 shows a half-section model of the furnace and a model of a concrete specimen with steel casing. Two oil burners, one horizontal and one vertical, enable the thermal exposure of the standard time-temperature curve (ISO 834) [30] till the end of the fire test. Thereby, the furnace temperature is measured by two thermocouples that are placed in a central position with a distance of 10 cm to the inner edge of the furnace wall. All test specimens are placed vertically in front of the same furnace opening with an area of 0.5 m × 0.5 m. Closing walls are placed in front of the other two openings of the furnace.

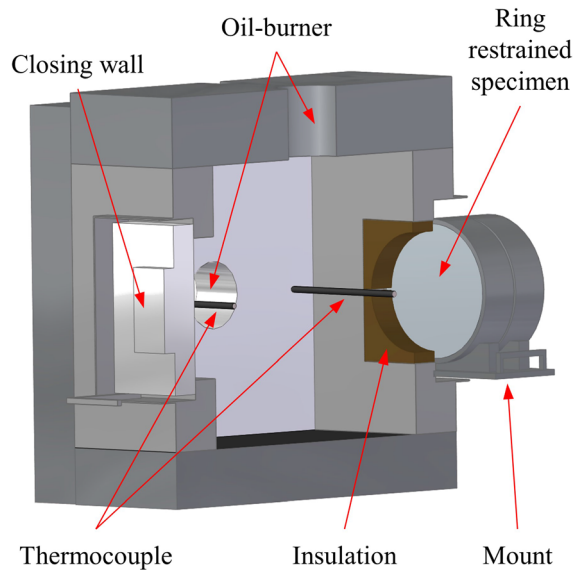

Fig. 1 Cutaway model of the test furnace including a vertical and a horizontal oil-burner and two thermocouples to regulate the fire curve. The ring restrained specimen is placed on a steel mount in front of the furnace opening

2.2 Specimens

The spalling behaviour of 8 unreinforced concrete specimens made of two ordinary concrete mixtures (Table 1) was investigated using three different specimen configurations (Fig. 2). The cuboid specimens, 0.6 m × 0.6 m × 0.29 m, as well as the concrete mixtures base on the previous research project [18]. Additionally, cylindrical specimens with the dimensions of Ø = 0.47 m, h = 0.29 m were tested unrestrained as well as restrained by two steel rings with an inner diameter of 0.492 m, a wall thickness of 8 mm and a height of 0.14 m (based on the developed test set-up described in [24, 31]). The steel rings were applied to restrain the thermal expansion of the concrete as well as to reduce the water loss over the shell surface. It was the aim to recreate the testing conditions in the centre of a large scale member. Thus, the test set-up of the cylindrical shaped specimens was adapted with insulation to shadow the steel rings from a direct heat input of the furnace (see sketch of Fig. 2). The furnace opening as well as the installation of the insulation resulted in a ratio of the shadowed area to the specimen size of 0.3 for the cuboid shaped specimens and the cylindrical shaped specimens including the steel rings. This set-up enables a lower thermal expansion of the steel compared to the concrete and therefore, a restrained expansion of the specimen. After casting, all

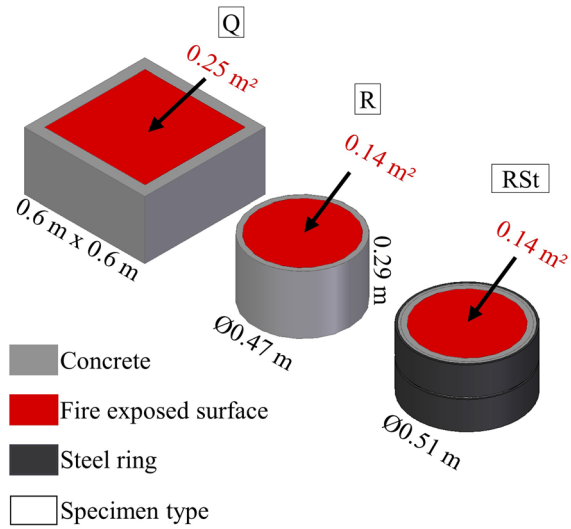

Fig. 2 Sketches of the three different specimen types

Table 1 Overview of the two concrete mixtures

Type of material	Ordinary concrete C5 Amount of components (kg/m^3)	Ordinary concrete C6
Cement (CEM I 42.5 R)	270	270
Water	175	175
Fly ash	80	80
Superplastiziser	2.7	2.7
Aggregates		
Sand (quartzitic)		
0 / 2 mm	536	536
Coarse grains	Quartzitic	Basalt
	Gravel	Grit
2 / 4 mm	285	513
4 / 8 mm	339	158
8 / 16 mm	624	711
28 d Cube		
Compressive	50	56
Strength (MPa)		
Fire curve	ISO834	ISO834

specimens cured in the formwork for one day. Afterwards, the specimen were stored in a sealed plastic foil at an air humidity of 100 % in the laboratory hall. Two weeks prior to the fire test, the plastic foil was removed and the specimens cured under laboratory climate conditions. Within these two weeks, the steel rings were applied to the specimens using an expanding mortar. A small gap of 10 mm between the steel rings was set as a heat barrier to reduce the heat transfer within the steel rings into deeper parts of the specimen. Before and after the fire tests, every specimen was scanned with a 3D scanning system. Fixed target points on the specimens ensure a good alignment

of the two digitalised surfaces. This allows the calculation of the spalling volume as well as the maximum spalling depth. Five embedded type-K sheath thermocouples in depths of 5 mm, 15 mm, 30 mm, 50 mm and 100 mm from the fire exposed surface measured the temperature inside the specimens during the fire test. For the restrained specimens, four thermocouples were welded on the steel rings in a distance of 1 cm from the fire exposed side to compare the steel temperature with the temperature of the specimen. Ten acoustic emission (AE) sensors (Vallen VS150-MS) were placed on the fire-unexposed reverse surface of the specimen to measure the mechanical waves that were transmitted into the specimen by spalling events and cracking. The use of acoustic emission sensors to measure and analyse cracking as well as spalling has been successfully implemented in previous studies [32–34]. The AE measuring system has a limited amount of capacity to record individual AE signals in a small time frame and it is assumed that spalling leads to high energy signals with high amplitudes. To minimise the risk of a detection overflow and to gather especially the signals from spalling events, the threshold amplitude was set to 60 dB to detect an AE signal as a hit. Additionally, a microphone was placed outside of the furnace to record all spalling events. After the fire test, the records of the microphone and the AE measurements were synchronised in time to separate spalling events and cracking in the AE data.

3 Results and discussion

The results of the air moisture measurements revealed that every specimen cured in an environment of 100 % air moisture content until the plastic foil was removed two weeks before the fire test. Thus, all specimens cured under the same conditions. The moisture content was determined by weight differences using cylindrical specimens ($Ø = 0.1$ m; $h = 0.3$ m) that were manufactured simultaneously and cured under the same conditions as the fire exposed specimens. The cylinders were dried at 105°C a week before the fire test in an electrical furnace. During the time, the small cylinders were weighted and further dried until the mass constant ($\Delta m \leq 0.1$ % within 24 h) was reached. The mean moisture content for the specimens with quartzitic aggregates was 5.1 % and 5.5 % for the specimens that contained basalt grit.

3.1 Surface damage

The results of the 3D scans are shown in Fig. 3 for the concrete with quartzitic aggregates (C5) and in Fig. 4 for the concrete with basaltic aggregates (C6). Table 2 shows an overview of the determined spalling volumes and maximum spalling depths from the 3D scanning results. All three different specimen types have different spalling behaviours. The fire exposed surface of the cuboid shaped specimens was reduced by 30 % (0.5 m × 0.5 m) compared to the previous research (0.6 m × 0.6 m) [18]. Thus, a shadowed rim occurred that caused an additional thermal gradient on the fire exposed surface. The results show that the surface damage was not significantly influenced by the shadowed area. Further, a positive residual elongation of the specimens towards the flame occurred in the centre of the fire exposed surface, whereas the boundary of the specimen has a negative residual elongation. Both elongations have values less than one millimetre and thus, have no significant influence on the calculation of the spalling volume. The macroscopic cracks (Fig. 5) on the fire exposed surface for the specimens C5-Q1 and C5-Q2 are a result of the reduction of the thermomechanical

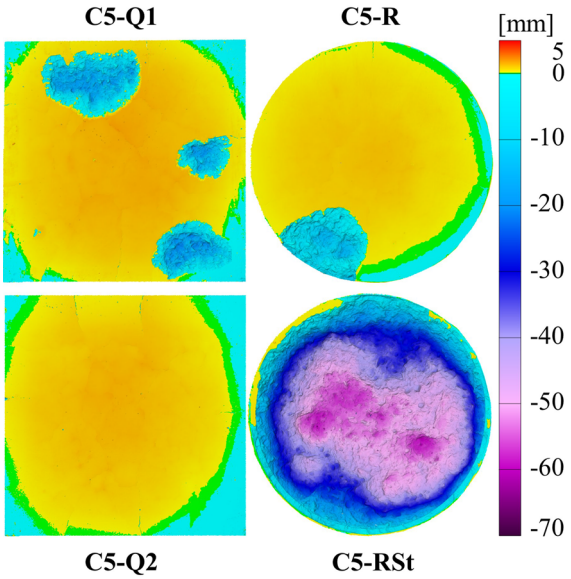

Fig. 3 Results of the 3D-Scans for every specimen of the concrete with quartzitic coarse aggregates (C5) after the fire test. The specimens Q1 and Q2 are unrestrained cuboids, R is an unrestrained cylindrical specimen and RSt is a restrained cylindrical specimen

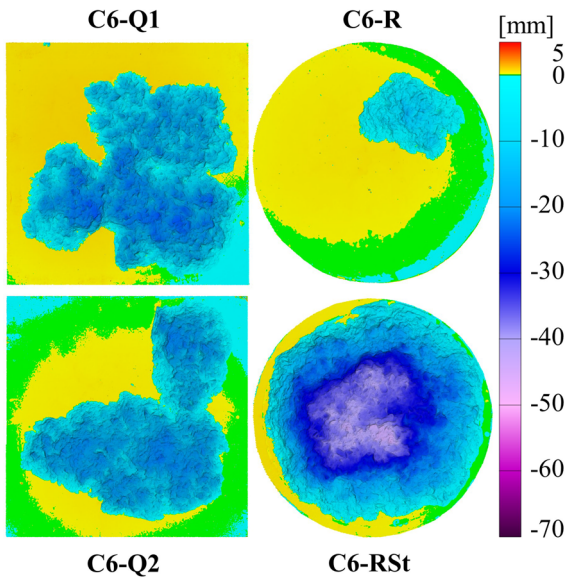

Fig. 4 Results of the 3D-Scans for every specimen of the concrete with basalt grit aggregates (C6) after the fire test. The specimens Q1 and Q2 are unrestrained cuboids, R is an unrestrained cylindrical specimen and RSt is a restrained cylindrical specimen

stresses. Those cracks connect the surface with the specimen sides and enhance the release of vaporised water, which leads to a reduction of thermohydraulic stresses. This results in only minor spalling with small areas on the fire exposed surface for specimen C5-Q1, for specimen C5-Q2 spalling is prevented. The basaltic aggregates of the specimens C6-Q1 and C6-Q2 have a lower thermal expansion compared to the quartzitic aggregates [7]. For this mixture, the number of macroscopic cracks was decreased compared to the mixture C5 (see Fig. 5) and resulted in an increase of the spalling volume (2.1 % for C6-Q1 and 2.0 % for C6-Q2) and maximum spalling depth in the centre of the fire exposed surface. Hence, spalling results from the combination of a slow build up of thermomechanical stresses and high thermohydraulical stresses due to less release of vaporised water. Further, spalling did not occur on the shadowed edge of the fire exposed specimen side for all cuboid shaped specimens of both mixtures. Thus, thermal induced stresses were released through cracking in this area. A reduction of the specimen size as well as the change of shape from cuboid (Q) to cylindrical (R) specimens lead to a similar spalling behaviour of both mixtures (compare Figs. 3 and 4). The specimen C5-R shows a similar spalling behaviour as the specimen C5-Q1, whereas the spalling volume of mixture C6 is halved (see Table 2). The reduced spalling volume of C6-R compared to C6-Q results from an increased water release by means of the macroscopic cracks as well as the smaller specimen size and therefore, lower thermomechanical stresses. In contrast to the previous discussed specimens, the application of steel rings to the cylindrical specimens led to a significant increase of thermomechanical stresses induced by the restrained expansion of the concrete. As a result, the specimens C5-RSt and C6-RSt have a higher spalling volume and larger maximum spalling depth. The restrained expansion of the specimen increased the thermomechanical stresses at the fire exposed surface compared to the unrestrained specimens. Additionally, the steel rings restrained the water loss through the side of the specimen, which also increased the thermohydraulic stresses. For mixture C5 the spalling volume increased from 0.8 % for the cylindrical, unrestrained

Table 2 Overview of the spalling depths and spalling volumes for all tested concrete specimens

Specimens		Spalling volume			Maximum spalling depth
		(dm^3)	(dm^3/m^2)	(%)	(mm)
C5 (quartzitic)	Q1	0.4	1.0	0.4	16
	Q2	–	–	–	–
	R	0.4	2.3	0.8	15
	RSt	6.1	35.1	12.1	63
C6 (basalt)	Q1	2.2	6.1	2.1	21
	Q2	2.1	5.7	2.0	20
	R	0.4	2.5	0.9	16
	RSt	3.4	19.7	6.8	45

The calculation of the spalling volume is related to the fire exposed area including the shadowed area (see Fig. 2).

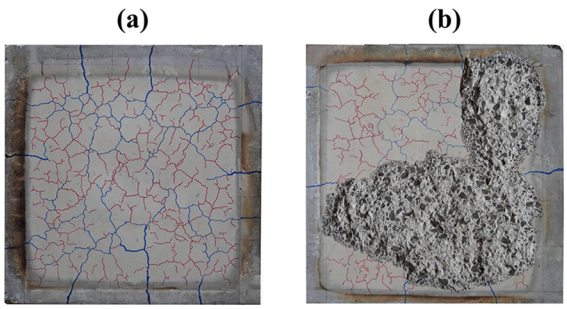

Fig. 5 Pictures of the fire exposed surface with highlighted macroscopic cracks of the cuboid shaped specimen with quartzitic gravel without spalling **a** and the cuboid shaped specimen with basalt grit with spalling **b** after the fire test

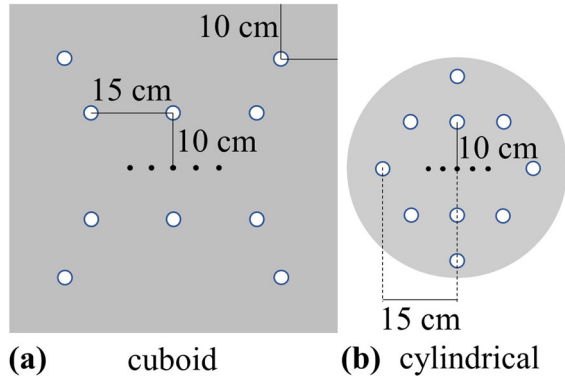

Fig. 6 Sketch of the acoustic emission sensor distribution on the backside of the **a** cuboid shaped specimen and **b** cylindrical specimen

specimen (C5-R) to 12.1 % for the cylindrical specimens with applied steel rings (C5-RSt) with a maximum spalling depth of 63 mm. Further, the spalling volume for C6-R is 0.9 % and 6.8 % for the ring restrained specimens (C6-RSt) with a spalling depth of 45 mm. The application of steel rings lead to a significant increase in the spalling of both concrete mixtures compared to the cuboid shaped specimens and unrestrained cylindrical specimens.

Due to the similarity of the concrete mixtures, it is assumed that the different spalling behaviours are mainly caused by the lower thermal expansion of the basaltic aggregates [7]. The spalling volume of C6-RSt is 44 % lower and the maximum spalling depth is reduced by 31 % compared to the specimen C5-RSt. For the same restrained testing conditions, the lower thermal expansion leads to reduced thermomechanical stresses and thus, to reduced spalling. On the other hand, the lower thermal expansion of the basalt reduced the occurrence of macroscopic cracks and led to larger spalling depths for the unrestrained specimens. The results of the 3D scans show that the test conditions of the specimens are an essential parameter for a comparison with the test conditions in the centre of a large member.

3.2 Time dependent damage

3.2.1 Temperature propagation and acoustic emission results

The results of the 3D scans are limited to the surface damage of the specimens and only provide information about the condition of the specimens before and after the fire test. Ten acoustic emission sensors were placed

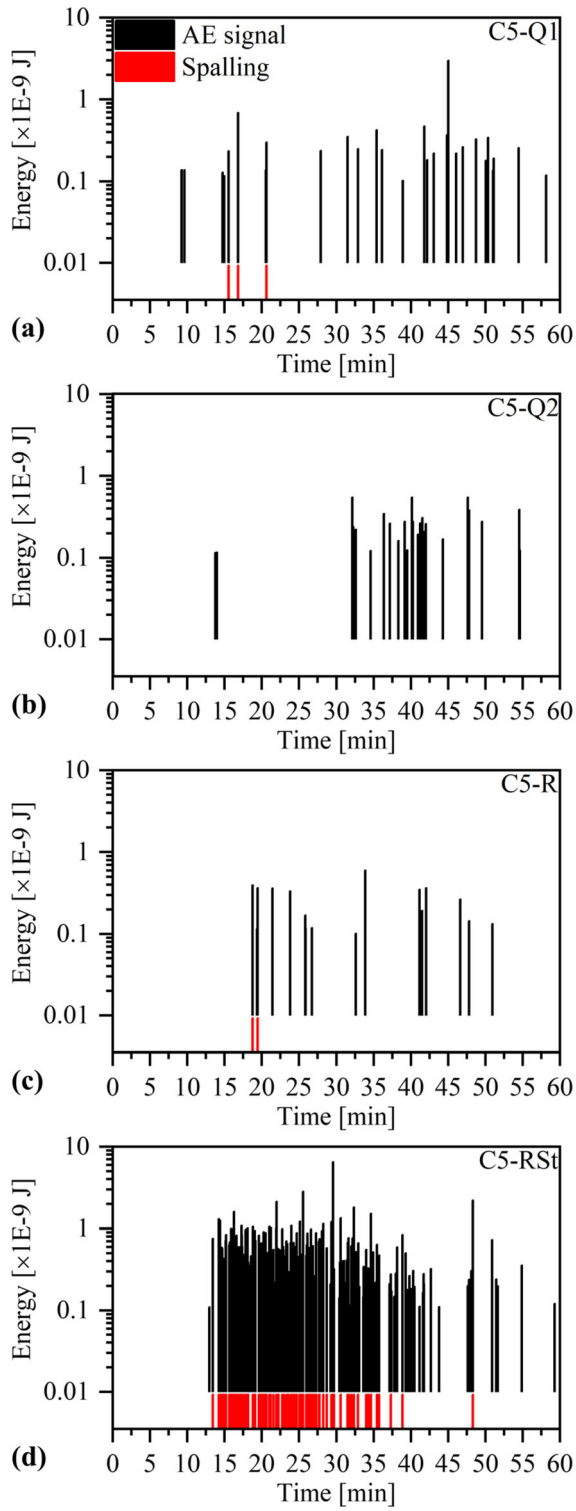

Fig. 7 Results of the acoustic emission (AE) measurements for every specimen of the concrete mixture with quartzitic aggregates. The energy of AE signals and their maximum energy are displayed over the testing time (black). The detected spalling events base on the audio recordings (red)

on the backside of the specimens to measure acoustic signals that were triggered by the formation of cracks inside the concrete during the fire test (Fig. 6).

The acoustic emission (AE) sensors measure different types of parameters for a detected event (hit) in dependence of the measuring time, i.e. the amplitude, the signal energy, the duration and the rise time of a signal. The gained data set is a combination of signals that were triggered by spalling and cracking inside the specimen. The connection of AE signals with a high energy level to spalling are described in [35]. These events are a result of a fast stress release inside a small volume near the fire exposed surface that induce high energetic acoustic waves into the concrete. Due to the large distance of up to 29 cm from the fire exposed surface to the AE sensors, the energy of the AE signals was damped strongly and the largest detected signal energies were between 10^{-09} J and 10^{-08} J. It was assumed that spalling events induce the largest signal energies. Thus, all recorded AE signals with the highest energy values (min. 10^{-10} J) are displayed in Figs. 7 and 9. In the study of Mróz et al. [36], the authors were able to precisely time the occurrence of spalling events using microphones. In our study, a microphone also recorded the sound including spalling events during the fire test. Afterwards, the spalling events in the recorded microphone data were aligned with the records of the AE sensors. In Figs. 7 and 9 the time of occurrence for verified spalling events from the microphone data are added as red bars. Further, Figs. 8 and 10 show the temperature distribution of the five embedded thermocouples in depths of 5 mm, 15 mm, 30 mm, 50 mm and 100 mm. Additionally, the steel ring temperature was measured in a depth of 1 cm from the fire exposed surface of specimens C5-RSt and C6-RSt during the fire test (Fig. 11). Considering the results of the 3D scans for the cuboid shaped specimens (see Sect. 3.1), the surfaces of the specimens of mixture C5 spalled less compared to the specimens surfaces of mixture C6. Only three spalling events occurred for specimen C5-Q1,

whereas specimen C5-Q2 did not spall (Table 3). Each of the three recorded spalling events in the microphone data correspond to an acoustic event with a high energy value above 10^{-10} J for the specimen C5-Q1 (Fig. 7a). Despite these three spalling events of C5-Q1, macroscopic cracks with a high energy occurred at similar times for C5-Q1 and C5-Q2 during the fire tests. Due to the intact concrete cover, the temperature increase within the specimens was not affected. The cuboid shaped specimens of mixture C6 (C6-Q1 and C6-Q2) have a larger spalling volume and a larger spalling depth compared to the same specimen type of mixture C5 (Table 2). Additionally, the spalling events occurred earlier and simultaneously to the acoustic events with energies above 10^{-10} J for these specimens. It is assumed that the low thermal expansion of basalt grit leads to a smaller amount of macroscopic cracks compared to mixture C5 (Fig. 3). Thus, the water loss is lower, which leads to high thermohydraulic induced tensile stresses and results in spalling. All AE events with energies above 10^{-10} J were detected simultaneously to the spalling events in the recorded data of the microphone. The last spalling event occurred after 21 min of fire exposure and afterwards, no AE signal with high energy was detected. Thus, the energy filter separates all occurring spalling events from the AE signals that were emitted by cracking for the specimens C6-Q1 and C6-Q2. As a result of spalling events, the embedded thermocouples were directly exposed to the fire at a depth of 5 mm. This led to a faster increase of the temperatures up to a depth of 30 mm. The embedded thermocouples in 50 mm and 100 mm depth from the fire exposed surface measured no significant temperature differences compared to the non-spalled cuboid shaped specimens of C5. The change of the geometry from cuboid shaped to cylindrical, unrestrained shaped specimens led to a more homogeneous expansion of the fire exposed surface (see Sect. 3.1). Two spalling events were detected for the specimen C5-R and C6-R, respectively. Additionally, AE signals with an energy level above 10^{-10} J were detected for each spalling event. For specimen with quartzitic aggregates (C5-R) seven crack-forming events were detected after the spalling ended, whereas no further high energy event was detected for specimen C6-R. However, the increased cracking of the specimen C5-R had no direct influence on the temperatures and both

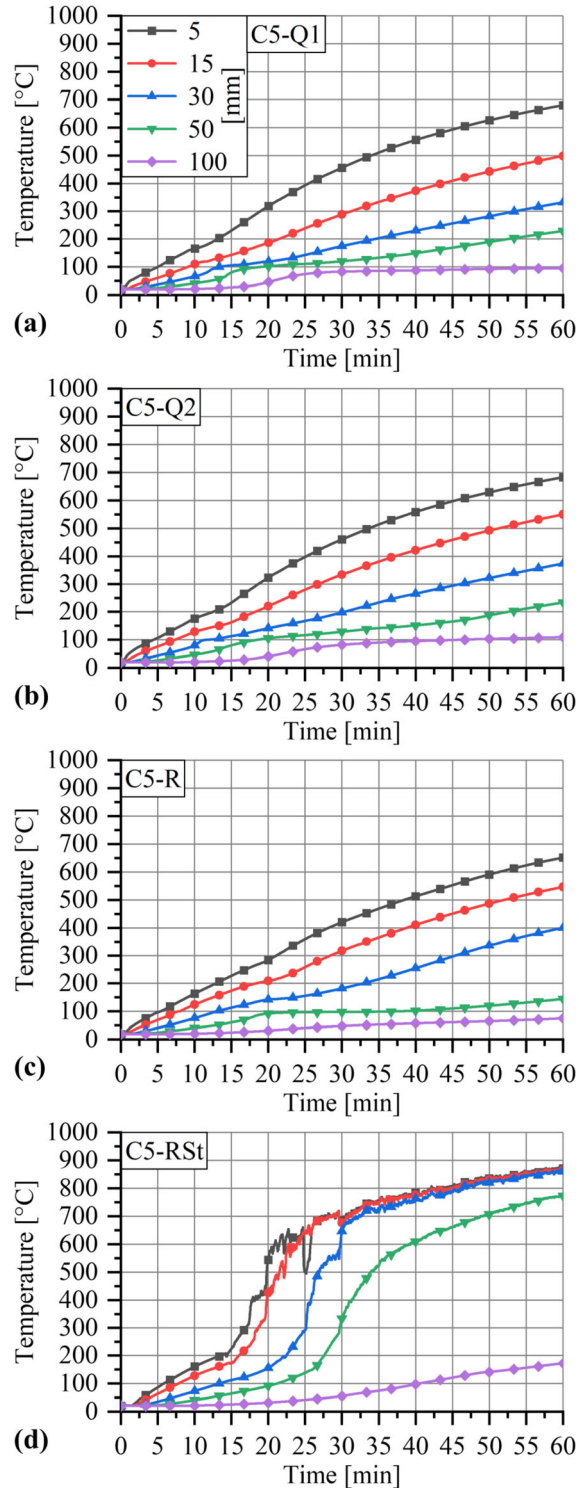

Fig. 8 Temperature profiles of the concrete mixture with quatzitic aggregates (C5) for **a** and **b** the cuboid shaped specimens, **c** the cylindrical, unrestrained specimen and **d** the cylindrical specimen with applied steel rings

Table 3 Number of measured AE events above 10^{-10} J and recorded spalling events of the audio data

Specimens		AE events (–)	Spalling events (–)
C5 (quartzitic)	Q1	28	3
	Q2	–	–
	R	16	2
	RSt	227	118
C6 (basalt)	Q1	6	6
	Q2	11	11
	R	2	2
	RSt	48	42

cylindrical, unrestrained specimens showed similar maximum temperatures at the end of the fire test. The restrained thermal expansion due to the application of steel rings as well as the restrained water loss increased the spalling volume of both mixtures significantly (Fig. 9). The temperatures of the steel rings at 1 cm from the fire exposed surface were always lower than the temperatures inside the concrete at 5 cm depth (compare Figs. 8, 10 and 11). Thus, the thermal expansion of the concrete is larger than the surrounding steel. As a result of the massive spalling of C5-RSt, the steel ring was partly exposed to the ISO 834 fire curve. This led to an enhanced increase of the steel temperature after 30–40 min of fire exposure. The temperature discrepancy induced thermomechanical stresses in the boundary zone of the fire exposed surface and resulted in an increased crack formation and spalling. For specimen C5-RSt 118 spalling events were detected in the audio data, whereas only 42 spalling events occurred for specimen C6-RSt (Table 3). For all these spalling events an associated AE signal above an energy level of 10^{-10} J was measured. Thus, all specimens of this study show a temporal correlation of detected spalling and high energy events in the AE data (Figs. 7 and 9). Further, the number of AE events not associated to spalling events increased for both steel ring restrained specimens. These events were caused by either macroscopic cracking or unrecorded spalling events in the audio data. The increased spalling volume of the ring restrained specimens compared to the unrestrained specimens led to a direct thermal exposure of the thermocouples up to a depth of 50 mm. Due to the reduced concrete covering, the temperature at a depth of 100 mm for C5-RSt was 70 °C higher compared to C5-R at the end of the fire test. For mixture C6 the temperature difference between the ring restrained and unrestrained specimen was 41 K. Thus, a larger spalling depth led to a faster temperature increase in larger depths of the specimens. The results show that the application of steel rings to the concrete specimen increases the overall damage of the specimens compared to the unrestrained specimens.

The adjustment of the intermediate scale specimens of the previous study [18] leads to a significant increase of the spalling volume and the spalling depth. Additionally, the ring restrained specimen of mixture C5 has a similar damage behaviour compared to the unrestrained, full scale specimen (1.8 m × 1.2 m × 0.3 m) of the same mixture (Table 4). Thus, the test set-up of the ring restrained specimens seems to be suitable for screening-tests.

4 Conclusions

The study shows the development of a screening-test method for intermediate scale specimens, taken into account the effect of a specimen size reduction. Based on the results of a previous research project at BAM [18] and the investigation of [24], the influence of restrained thermal expansion on the spalling behaviour is investigated on two similar, ordinary concrete mixtures using unreinforced specimens. The susceptibility to spalling was investigated for unrestrained, cuboid shaped specimens as well as unrestrained and restrained, cylindrical shaped specimens. In contrast to the previous research, the specimens were tested in a different furnace, which led to a reduction of the fire exposed surface of 30 % and a shadowed edge for the cuboid shaped

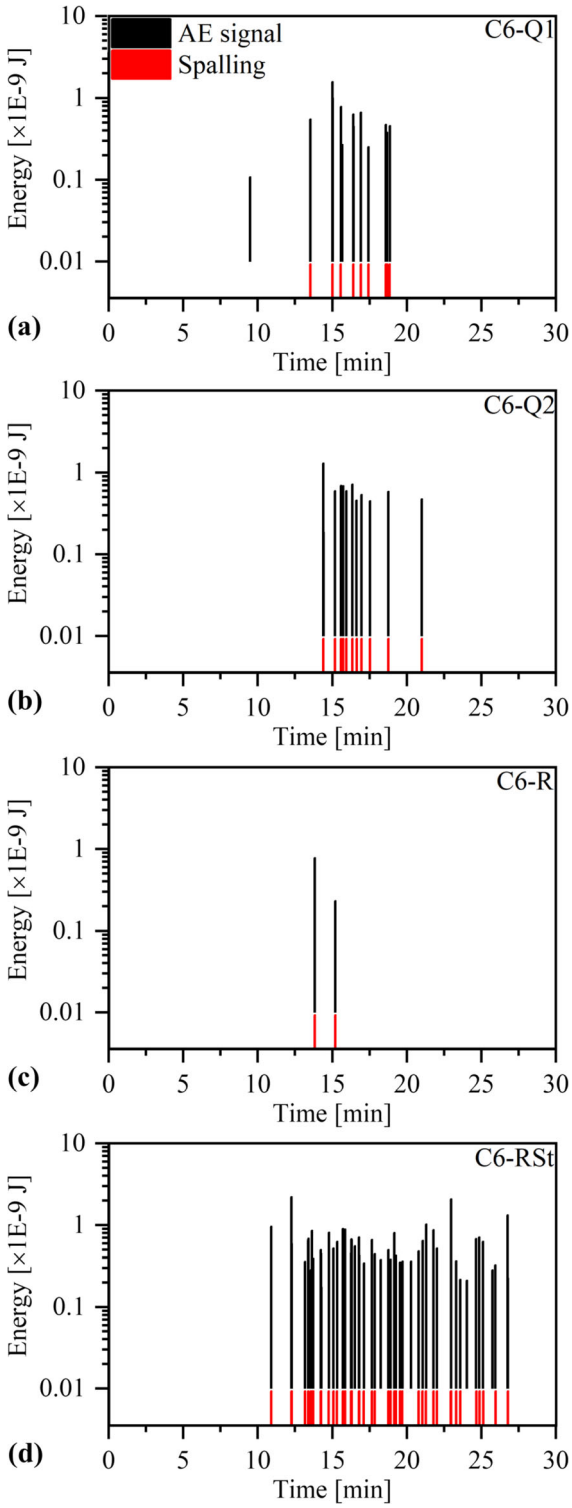

◀**Fig. 9** Results of the acoustic emission (AE) measurements for every specimen of the concrete mixture with basalt grit. The energy of AE signals and their maximum energy are displayed over the testing time (black). The detected spalling events base on the audio recordings (red)

specimens. Due to the smaller specimen size of the cylindrical, steel ring restrained specimens, an insulation was applied to protect the steel from a direct heat input. Additionally, the fire exposed surface of the cylindrical specimens was reduced in relation to the reduced specimen size compared of the cuboid shaped specimens by the insulation. The results show that the reduced fire exposed surface has no significant influence on the spalling behaviour of the specimens. The cuboid shaped specimens with quartzitic aggregates showed little to no spalling, whereas the specimens with basaltic aggregates showed increased spalling. The larger thermal expansion of the quartzitic aggregates and unrestrained specimen set-up led to a release of thermomechanical stresses through cracking in the boundary zone of the fire exposed surface. Vaporised water was released from deeper parts of the specimen through macroscopic cracks at the specimen side. On the other hand, the low thermal expansion of the basalt led to reduced cracking and reduced water loss compared to the quartzitic aggregates. Thus, thermohydraulic induced stresses are increased and released through spalling for the cuboid shaped specimens. The results of the unrestrained, cylindrical shaped specimens show a similar spalling behaviour for both concrete mixtures. The smaller specimen size and the cylindrical shape of the specimens led to an increase of boundary effects. Macroscopic cracks connected the fire exposed surface and the side of the specimens. This led to a release of vaporised water and thus, spalling occurred similarly for both mixtures. The type of aggregate has no direct influence on the spalling behaviour for this specimen type. The application of steel rings on the cylindrical shaped specimens led to a significant increase of the spalling volume and spalling depth for both mixtures. The restrained thermal expansion of the concrete and reduced water loss at the specimen side increased the

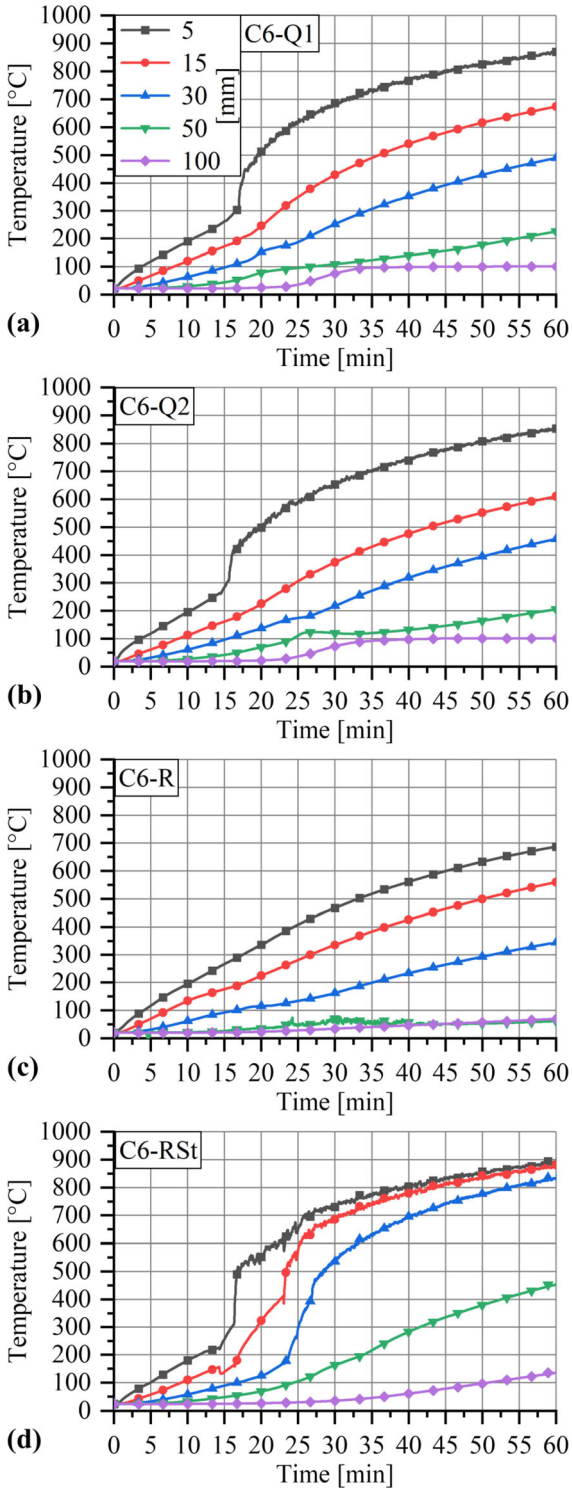

Fig. 10 Temperature profiles of the concrete mixture with coarse basalt aggregates (C6) for **a** and **b** the cuboid shaped specimens, **c** the cylindrical, unrestrained specimen and **d** the cylindrical specimen with applied steel rings

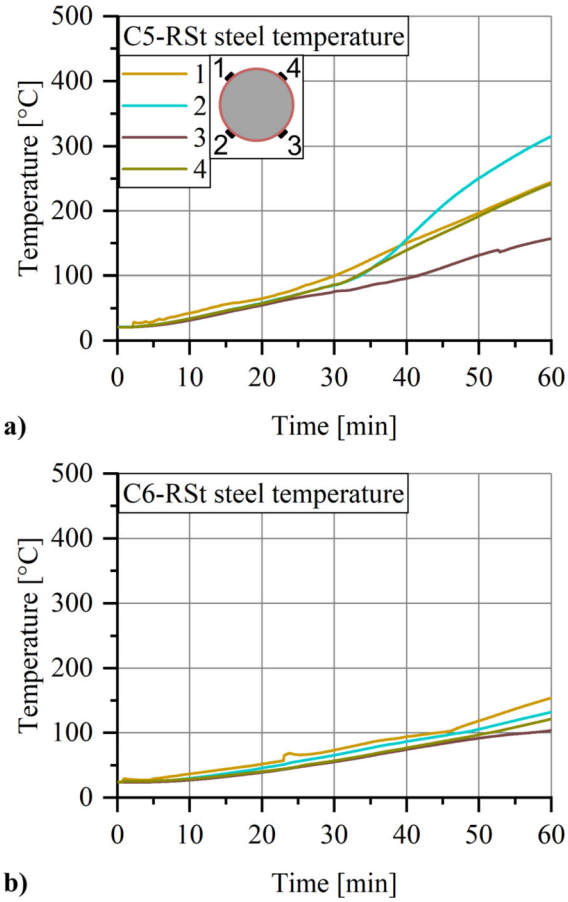

Fig. 11 Steel ring temperature for the cylindrical and restrained specimen with **a** quartzitic aggregates and **b** basalt grit

thermomechanical as well as thermohydraulic induced stresses in the boundary zone of the fire exposed surface and as a consequence led to increased spalling. For this specimen type a larger spalling volume was measured for the specimen with quartzitic aggregates compared to the specimen with basalt. The results of the acoustic emission measurements and the recorded audio data show that the number of spalling events is significantly lower for the unrestrained specimens. Further, the specimens containing quartzitic aggregates show a larger number of high-energy AE events without spalling due to crack formation. The amount of spalling events increases with the restrained thermal expansion of the concrete. Additionally, the number of high-energy events that occurred without spalling in the audio data, is almost twice as high as the amount of spalling

Table 4 Comparison of the spalling depths and spalling volumes for the full scale (1.8 m × 1.2 m × 0.3 m) and intermediate scale (0.6 m × 0.6 m × 0.3 m) concrete specimens of the previous study [18] and the ring restrained specimen of the same concrete mixture

Specimens		Spalling volume		Maximum spalling depth
		(dm^3/m^2)	(%)	(mm)
C5 (quartzitic)	Full scale	25.8	8.6	76
	Intermediate scale	6.1	2.0	39
	RSt	35.1	12.1	63

events for the restrained specimen with quartzitic aggregates. On the other hand, the number of high-energy acoustic events almost matches the number of spalling events for the same specimen type with basaltic aggregates. Thus, the type of aggregate and its thermal expansion have a direct influence of the spalling behaviour for the unrestrained, cuboid shaped and the ring restrained specimens.

The study shows that the application of steel rings increases the spalling of a concrete mixture compared to the unrestrained specimens. In comparison to the previous study [18], the spalling results of the specimen with a restrained expansion are similar to the results of a large scale member. Thus, this type of specimen seems to be suitable to investigate the susceptibility to spalling on a material scale (screening-tests).

Acknowledgements The authors gratefully acknowledge the employees of the Division of Fire Engineering, the Division of Building Materials and Division of Technology of Construction Materials at BAM that were part of this study for their support.

Declarations

Conflict of interest The authors authors have no relevant financial or non-financial interest to disclose.

References

1. Hertz KD (2003) Limits of spalling of fire-exposed concrete. Fire Saf J 38:103–116
2. Cruz CR, Gillen M (1980) Thermal Expansion of portland cement paste, mortar and concrete at high temperatures. Fire Mater 4:66–70
3. Harmathy TZ (1965) Effect of moisture on the fire endurance of building elements. Am Soc Test Mater Spec Tech Publ 385:74–95
4. Stelzner L, Powierza B, Tyler O, Dlugosch R, Weise F (2019) Thermally-induced moisture transport in high performance concrete studied by X-ray-CT and 1H-NMR. Constr Build Mater 224:600–609
5. Jansson R, Boström L (2009) Fire spalling—the moisture effect. In: 1st International RILEM workshop on concrete spalling due to fire exposure, Leipzig
6. Jansson R, Boström L (2013) Fire spalling—the moisture effect, part II. In: MATEC Web of Conferences 6. https://doi.org/10.1051/matecconf/20130603003
7. Schneider U (1982) Behaviour of concrete at high temperatures. Deutscher Ausschuss für Stahlbeton 337
8. Salmang, H, Scholze, H (1968) Keramisch wichtige Systeme. In: Die physikalischen und chemischen Grundlagen der Keramik, 162. Springer, Berlin, Heidelberg
9. Pimienta P, Hager I (2002) Mechanical behaviour of HPC at high temperature. In: 6th international symposium on utilization of high strength/high performance concrete, Leipzig
10. Bosnjak J, Sharma A, Grauf K (2019) Mechanical properties of concrete with steel and polypropylene fibres at elevated temperatures. Fibers 7:1–13. https://doi.org/10.3390/fib7020009
11. Siemon M, Zehfuß J (2018) Behaviour of structural elements exposed to fire and mechanical loading. J Struct Fire Eng 8:138–146. https://doi.org/10.1108/JSFE-01-2017-0020
12. Dehn F, Werther N, Knitl J (2006) Großbrandversuche für den City-Tunnel Leipzig. Beton- und Stahlbetonbau 101 (8):631–636. https://doi.org/10.1002/best.200608186
13. Boxheimer S, Knitl J, Dehn F (2009) Fire tests on precast tunnel segments for the liefkenshoekspoortunnel in Antwerp. In: 1st International RILEM workshop on concrete spalling due to fire exposure, Leipzig
14. Guerrieri M, Sanabria C, Lee WM, Pazmino E, Patel R (2020) Design of the metro tunnel project tunnel linings for

fire testing. Struct Concr 21:2452–2480. https://doi.org/10.1002/suco.202000140
15. Werner S, Rogge A (2015) The effect of various fire-exposed surface dimensions on the spalling of concrete specimens. Fire Mater 39:545–556
16. Zhao R, Sanjayan JG (2009) Test method for concrete spalling using small electric furnace. Fire Mater 34:189–201. https://doi.org/10.1002/fam.1020
17. Hertz KD, Sørensen LS (2005) Test method for spalling of fire exposed concrete. Fire Saf J 40:466–476
18. Klimek A, Stelzner L, Hothan S, Rogge A (2022) Fire induced concrete spalling in combination with size effects. Mater Struct 55:216
19. Mohd Ali AZ, Sanjayan J, Guerrieri M (2018) Specimen size, aggregate size, and aggregate type effect on spalling of concrete in fire. Fire Mater 42:59–68
20. Guerrieri M, Fragomeni S (2016) Mechanisms of spalling in concrete panels of different geometry in hydrocarbon fire. J Mater Civ Eng 12:1–12. https://doi.org/10.1061/(ASCE)MT.1943-5533.0001680
21. Hager I, Mróz K, Tracz T (2018) Concrete propensity to fire spalling: testing and observations. In: MATEC web of conferences 163. https://doi.org/10.1051/matecconf/201816302004
22. Mindeguia JC, Pimienta P, Noumowé A, Kanema M (2010) Temperature, pore pressure and mass variation of concrete subjected to high temperature—experimental and numerical discussion on spalling risk. Cem Concr Res 40:477–487
23. Boström L, Wickström U, Adl-Zarrabi B (2007) Effect of specimen size and loading conditions on spalling of concrete. Fire Mater 31:173–186
24. Ozawa M, Tanibe T, Kamata R, Uchida Y, Rokugo K, Parajuli SS (2018) Behaviour of ring-restrained high-performance concrete under extreme heating and development of screening test. Constr Build Mater 162:215–228
25. Stelzner L (2021) Analyse des thermisch induzierten Feuchtetransports in gefügedichten Betonen. Dissertation, Universität Stuttgart
26. McNamee R, Sjöström J, Biström L (2021) Reduction of fire spalling of concrete with small doses of polypropylene fibres. Fire Mater 2021:1–9. https://doi.org/10.1002/fam.3005
27. Pistol K, Weise F, Meng B (2012) Polypropylen-Fasern in Hochleistungsbeton. Beton- und Stahlbetonbau 107:476–483
28. Okrusch M, Matthes † S (2010) Einführung und Grundbegriffe. In: Mineralogie. Springer-Lehrbuch. Springer, Berlin, Heidelberg
29. Mohaine S, Boström L, Lion M, McNamee R, Robert F (2019) Cross-comparison of screening tests for spalling of concrete. Fire Mater 2021:1–14. https://doi.org/10.1002/fam.2946
30. Eurocode 1: Actions on structures - Part1-2: General actions - Actions on structures exposed to fire; German version EN 1991-1-2:2002 (2010)
31. Tanibe T, Ozawa M, Kamata R, Sato R, Rokugo K (2013) Thermal stress estimation in relation to spalling of HSC restrained with steel rings at high temperatures. In: MATEC web of conferences 6. https://doi.org/10.1051/matecconf/20130601004
32. Ozawa M, Uchida S, Kamada T, Morimoto H (2012) Study of mechanisms of explosive spalling in high-strength concrete at high temperatures using acoustic emission. Constr Build Mater 37:621–628
33. Grosse C, Richter R, Ožbolt J, Dehn F, Juknat M (2011) Spalling of HPC evaluated by acoustic emission and numerical analysis. In: 2nd international RILEM workshop on concrete spalling due to fire exposure, Delft
34. Huismann S (2010) Materialverhalten von hochfestem Beton unter thermomechanischer Beanspruchung. Dissertation, Technische Universität Wien
35. Richter R (2019) Anwendung der Schallemissionsanalyse bei Tunnelbrandprüfungen an Beton. Dissertation, Technische Universität München
36. Mróz K, Hager I (2021) Evaluation of nature and intensity of fire concrete spalling by frequency analysis of sound records. Cem Concr Res. https://doi.org/10.1016/j.cemconres.2021.106539